Noble gases and microporous frameworks; from interaction to application

A. Soleimani Dorcheh [a,c], D. Denysenko [b], D. Volkmer [b], W. Donner [c], M. Hirscher [a,*]

[a] Max-Planck-Institut für Intelligente Systeme, Heisenbergstr. 3, 70569 Stuttgart, Germany
[b] Institute of Physics, Augsburg University, 86135 Augsburg, Germany
[c] Department of Materials Science, Technische Universität Darmstadt, Petersenstr. 23, Darmstadt 64287, Germany

1. Introduction

Microporous frameworks have been extensively studied owing to their promising properties and tunable structures. Recent novel developments of coordination polymers resulted in several classes of microporous frameworks (MFs) including Metal–Organic Frameworks (MOFs), Covalent-Organic Frameworks (COFs) and Zeolite Imidazolate Frameworks (ZIFs). These new classes of microporous materials possess unique properties such as high specific surface area, high porosity and high thermal stability. They have a highly developed porosity that can be tuned by selection of different secondary building units (SBUs), different linkers or functionalizing their structures. Owing to their diverse and unique properties, they already created a strong interest for applications in hydrogen storage, methane storage, gas separation, catalysis, biology [1–6].

Recently, xenon (Xe) and krypton (Kr) have attracted a major attention of the industry and research owing to their special physiochemical properties. They are used in several industrial applications such as fluorescent light bulbs, excimer laser industry and magnetic resonance imaging (MRI) [7].

However, the high demand of these gases in above mentioned applications and the fact that there is no source of xenon and krypton richer than air containing only 1 ppm of krypton and 0.08 ppm of xenon causes the high cost of these gases. Up to now, krypton and xenon were produced as byproduct of the fractional air distillation process. After a set of enrichment cycles, their mixture must be purified and separated through further cryogenic distillation [8]. This procedure is time and energy intensive. Thus, a separation method at room temperature is demanded. Using adsorbents for separation and storage of krypton and xenon can be a substitution method for cryogenic distillation methods. There is an urgent need for the design and development of adsorbent materials for this application. There are several investigations described in literature applying charcoal and zeolites for noble gas adsorption and separation [9,10]. Recently, in a computational study, Ryan et al. investigated the separation of xenon and krypton in several MOF structures [11]. However, in order to go one step further toward application, it is necessary to experimentally investigate the interaction between the adsorbents and noble gases. Very recently, Thallapally et al. reported their findings in applying MOFs (NiDOBDC) for Xe/Kr separation [12].

In this work thermal desorption spectroscopy and adsorption isotherm are employed to study the adsorption of xenon and krypton in several MFs and their separation capability. The results show the potential candidates for this application.

2. Experimental

Four samples from three classes of MFs have been selected as following. HKUST-1 was provided by BASF as Basolite C300 produced via electrochemical method. The synthesis procedure is explained in reference [13]. MFU-4*l* is synthesized via solvothermal synthesis as explained in reference [14]. ZIF-8 was provided by BASF as Basolite Z-1200 [15]. COF-102 was synthesized by Fischer's

* Corresponding author. Tel.: +49 711 689 1808; fax: +49 711 689 1952.
E-mail addresses: soleimani@dechema.de (A. Soleimani Dorcheh), dmytro.denysenko@physik.uni-augsburg.de (D. Denysenko), dirk.volkmer@physik.uni-augsburg.de (D. Volkmer), wdonner@tu-darmstadt.de (W. Donner), hirscher@mf.mpg.de (M. Hirscher).

group[1] as explained in reference [16]. Krypton and xenon were purchased in high purity (99.9(4)%) from Westfalen GmbH.

Thermal desorption spectroscopy (TDS) was used to characterize the adsorbate–adsorbent interactions. An in-house designed apparatus formerly employed for hydrogen and deuterium [17] was modified for measuring noble gas desorption. The principles of the experiment are explained in [18]. Only a small amount of material (3–5 mg) was used for the TDS measurements in order to keep the evolution in the linear operational range of the mass spectrometer and to avoid readsorption [19]. Prior to exposing the samples to the noble gases, the material was outgassed at 423 K in high vacuum to remove all adsorbed gas species from the surface. TDS spectra were measured separately for krypton and xenon. The experimental conditions such as outgassing, loading pressure, loading temperature, cooling temperature and time intervals were kept similar for all measurements enabling a direct comparison of the results between krypton and xenon and for different samples. During the TDS measurements, the mass numbers of 18 (water), 28 (nitrogen), 84 (krypton) and 129 (xenon) were monitored simultaneously. It should be noted that since the desorption signal for xenon and krypton is not calibrated, the desorption rates are provided in arbitrary units. However, for each individual gas the spectra are presented in equal scale allowing a direct comparison of the samples.

The best candidates according to the TDS results were further investigated by isothermal adsorption and calculation of isosteric heat of adsorption. The samples were outgassed for 20 h at 200 °C before the first measurement and for 2 h at 150 °C between the measurements under high vacuum ($P < 10^{-4}$ mbar). Adsorption isotherms were measured with a BELSORP-max instrument combined with a BELCryo system. Argon adsorption isotherms for the determination of BET surface area were measured at 87.3 K. Krypton and xenon saturation adsorption isotherms were measured at 119.93 and 165.1 K, respectively.

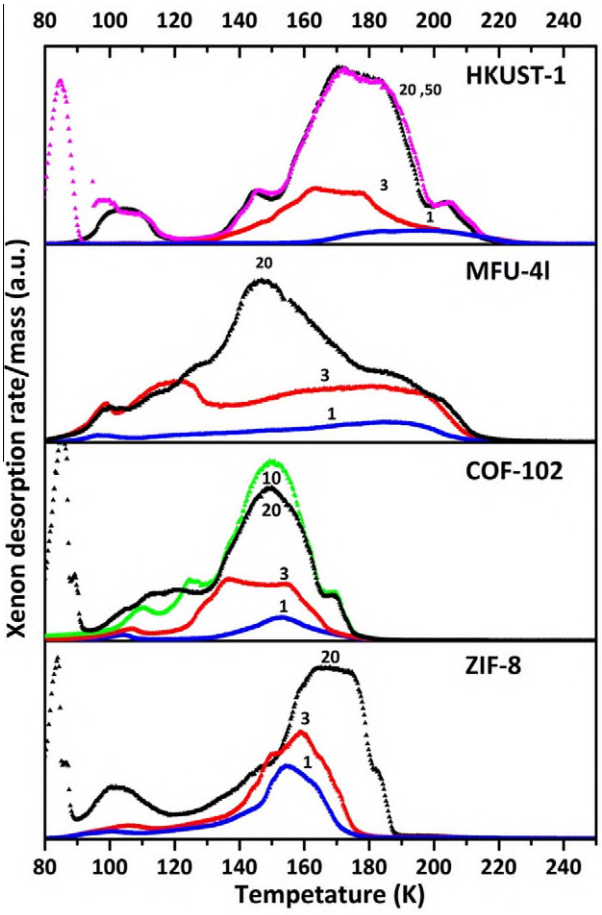

Fig. 1. Xenon desorption spectra of different MFs (Heating rate = 0.1 K s^{-1}). The different curves for each material correspond to different loading pressures as indicated by numbers giving the values in mbar.

3. Results and discussion

Figs. 1 and 2 show the xenon and krypton desorption spectra of the microporous frameworks, respectively. For each material several desorption spectra were measured after exposure to different loading pressures. Each sample demonstrates a characteristic desorption profile according to the interaction between its microporous structure and noble gas.

The temperature, at which all adsorbed gas atoms are desorbed (final desorption temperature, T_{Fin}), diversely represents the maximum strength of interaction between the adsorbents and adsorbate. Furthermore, the total amount of desorbed gas (the area under the spectrum) can be directly correlated to the uptake at the corresponding loading pressure.

For low loading pressure (P_L = 1 mbar) the xenon desorption spectra of all samples exhibit only a maximum in the high temperature region, i.e. above 120 K (Fig. 1). By increasing the loading pressure further, the intensity of the spectrum increases in the high temperature region and new desorption maxima are observed at temperatures below 120 K. In HKUST-1, MFU-4*l* and COF-102, the final desorption temperature is the same for all loading pressures, while in ZIF-8, T_{Fin} is increasing with loading pressure. It should be further noticed that T_{Fin} in HKUST-1 and MFU-4*l* is significantly higher than in COF-102 and ZIF-8. Fig. 2 shows the same experiments using krypton. In general, the krypron desorption spectra are shifted to low temperature compared to xenon. For higher loading pressure, additional maxima or shoulders appear at temperatures below 100 K. Again the final desorption temperature (T_{Fin}) is independent on loading pressure except for ZIF-8.

The desorption spectra can be divided in two temperature regions: a high temperature region is above 120 and 100 K for xenon and krypton, respectively and low temperature region below these temperatures. The low temperature region can be attributed to a part of xenon or krypton condensed at the exterior surface of the powder, since it is very close to the boiling points of the xenon and krypton (considering the experimental condition). No adsorption is observed in this region for lower loading pressure, since all the gas is adsorbed in the internal pore structure.

The desorption maxima in the high temperature region are correlated to the structure of the MFs. For each sample several desorption maxima are observed at different temperatures which can be correlated to different desorption energies provided by different sites in the MFs. Sequential filling of the adsorption sites at different loading pressure shows that at the lowest coverage (P_L = 1 mbar), noble gas atoms prefer to approach the strongest site with the highest adsorbent–adsorbate interaction. An increase in loading pressure leads to saturation of the preferential sites and new maxima at low temperature appear in desorption spectrum indicating an occupation of the weaker sites.

For applications of microporous materials in gas storage, especially for hydrogen storage, the maximum gas uptake is of the greatest importance. According to the former studies in porous materials, there is a direct relation between BET specific surface area (SSA) and saturation hydrogen uptake which is independent on structure and composition of the materials [20].

[1] Inorganic Chemistry II, Ruhr-University Bochum.

Considering similar experimental conditions (P_L = 20 mbar and T' = 0.1 K s^{-1}), the relation between the uptake and SSA of the studied MFs is illustrated in Fig. 3 for each gas. The area of the low temperature region of the spectra is not taken into account, since this area is not correlated to the gas uptake of the materials.

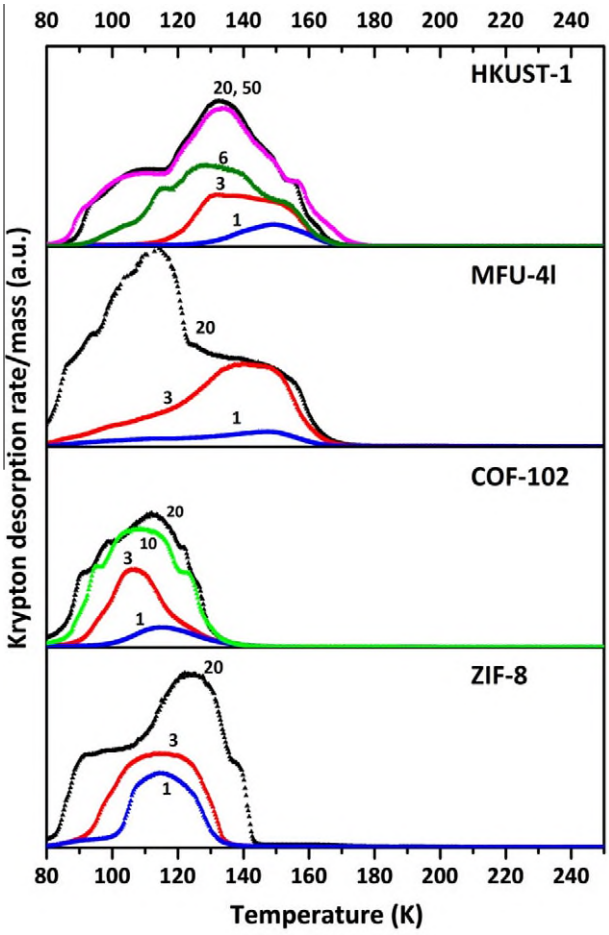

Fig. 2. Krypton desorption spectra of different MFs (Heating rate = 0.1 K s^{-1}). The different curves for each material correspond to different loading pressures as indicated by numbers giving the values in mbar.

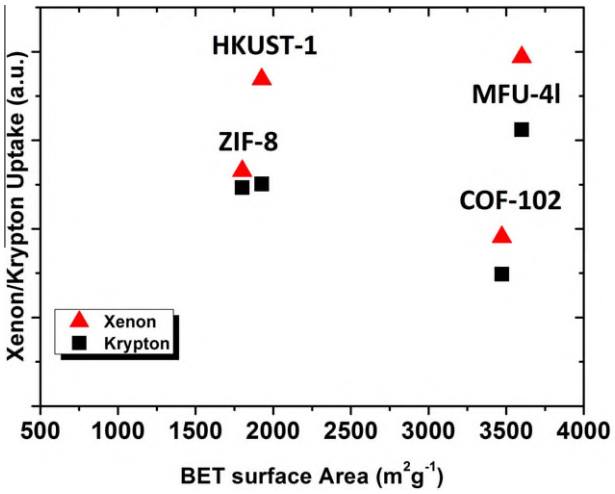

Fig. 3. The relation between the uptake (area under the spectra after loading at P = 20 mbar and heating rate = 0.1 K s^{-1}) and SSA.

The crystal structures of MFU-4*l*, HKUST-1, ZIF-8 and COF-102 are well described in references [14,17,21–23]. As Fig. 3 demonstrates, MFU-4*l* represents the highest uptake for both xenon and krypton compared to other samples. Although its SSA is higher, COF-102 show significantly less uptake compare to HKUST-1. Compare to other structures, MFU-4*l* provides larger pore and aperture sizes providing a more accessible structure to noble gas atoms.

According to Fig. 3, it can be implied that in contrast to hydrogen, the krypton and xenon uptake is not independent of the structure of the MFs. The kinetic diameter of the xenon and krypton are 3.96 and 3.6 Å, respectively, which is significantly larger than the corresponding value for hydrogen (2.89 Å). In addition, the boiling temperatures of xenon and krypton are higher than for hydrogen. Accordingly, the penetration of the noble gases into the MF structures at low temperature can be hindered and be dependent on the size of the apertures and the pores in the MF structure.

Although the storage capacity is an important adsorption property, the adsorption strength cannot be underestimated, especially for gas separation. For all investigated frameworks, desorption of krypton and xenon takes place in the temperature range between 77–180 and 77–226 K, respectively. At higher temperatures the amount of desorbed noble gas is negligible. Fig. 4 compares the final desorption temperature (T_{Fin}) of all samples for krypton and xenon. The difference in final desorption temperature can show the ability of the material to adsorb selectively a preferred gas from a gas mixture. Fig. 4 indicates that for all samples xenon possesses a higher final desorption temperature than krypton. This means that under equal pressure and temperature conditions, xenon will be favorably adsorbed over krypton. However, the difference between final desorption temperature of xenon and krypton depends on the material and can be used as a parameter for the preferential adsorption. This temperature difference is 51, 50, 40 and 44 K for HKUST-1, MFU-4*l*, COF-102 and ZIF-8, respectively. Higher desorption temperature of xenon in all samples can be due to the higher polarizability of xenon (α = 4.04 Å^3) versus krypton (α = 2.8 Å^3) [24] possessing higher interaction potential and consequently higher enthalpy of adsorption. In a systematic study, Farrusseng et al. measured the heats of adsorption of krypton and xenon in three MOF structures [24]. Their results show for all studied MOFs, including HKUST-1, that the heat of adsorption of xenon is higher than the one of krypton.

Considering the difference in final desorption temperature of the frameworks and their uptakes (Figs. 3 and 4), HKUST-1 and MFU-4*l* exhibit highest uptake as well as the highest tendency to adsorb xenon over krypton.

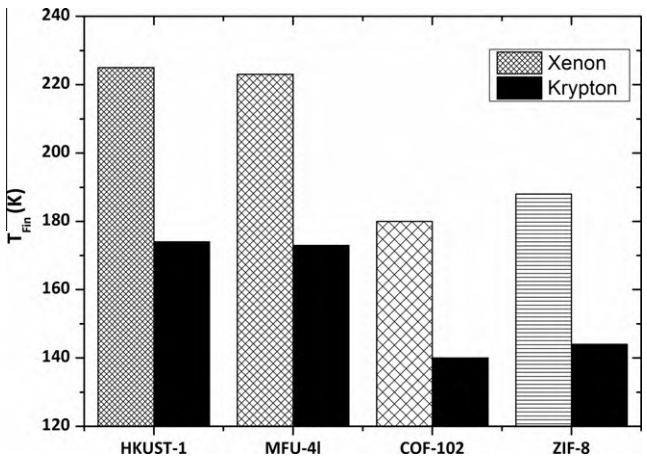

Fig. 4. Maximum desorption temperature of krypton and xenon for the studied MFs.

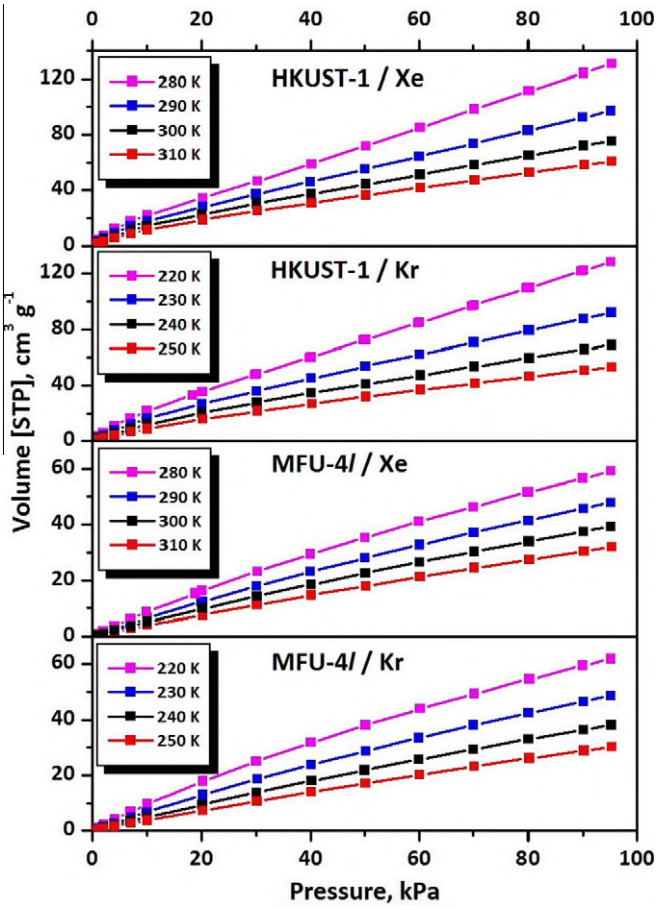

Fig. 5. Adsorption isotherms of Kr and Xe in MFU-4*l* and HKUST-1 at different temperatures.

For the determination of isosteric heats of adsorption in HKUST-1 and MFU-4*l*, four isotherms at 220, 230, 240 and 250 K for krypton and 280, 290, 300 and 310 K for xenon were measured (Fig. 5).

The isosteric heats of adsorption were calculated from the measured isotherms using the Clausius–Clapeyron Eq. (1). The complete calculation procedure is presented in the supporting information.

$$\Delta H = R\left(\frac{\partial(\ln P)}{\partial(1/T)}\right)_{\theta} \quad (1)$$

Krypton and xenon isosteric heats of adsoption at zero limit surface coverage ($Q_{st}{}^{0}$) are listed in Table 1. According to Table 1, at very low coverage (Henry's law region) the difference in isosteric heat of adsorbtion of Xe and Kr is 4.3 and 8.2 kJ mol^{-1} for MFU-4*l* and HKUST-1, respectively.

However, isosteric heat of adsorption is a function of surface coverage. The dependence on loading is shown in Fig. 6. It can be seen, that although HKUST-1 shows a higher Xe enthalpy of adsorption, it is rapidly decreasing in the loading range 0–1.5 mmol g^{-1} and remains almost constant at higher loadings. In contrast, for MFU-4*l* enthalpies of adsorption for both, Kr and Xe,

Table 1
Isosteric heats of adsorption at zero limit surface coverage.

	$Q_{st}{}^{0}$ (Kr), kJ mol^{-1}	$Q_{st}{}^{0}$ (Xe), kJ mol^{-1}
MFU-4*l*	15.7	20
HKUST-1	18.7	26.9

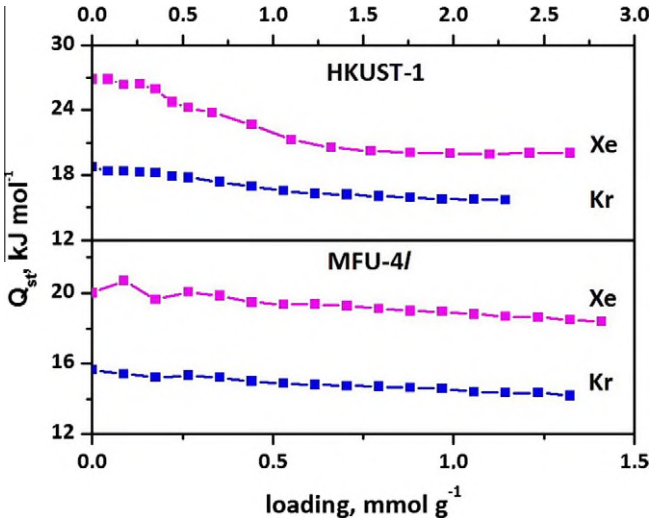

Fig. 6. Isosteric heats of adsorption of Kr and Xe in MFU-4*l* and HKUST-1 as a function of loading.

Table 2
Selectivity for the adsorption of Xe over Kr at very low surface coverage.

	280 K	310 K
MFU-4*l*	5.6	4.7
HKUST-1	11.8	8.4

decrease slowly with increasing loading. The enthalpy of adsorption for Kr in HKUST-1 decreases with increasing loading as well, however not as fast, as for Xe. At higher surface coverage, the difference in Xe and Kr enthalpy of adsorption remains almost constant.

The maximal selectivity of adsorption can be obtained from Henry constants: $S_{Xe/Kr} = K_H(Kr)/K_H(Xe)$. Table 2 shows the selectivities for the adsorption of Xe over Kr at very low surface coverage, calculated for two different temperatures. In the case of Kr, Henry constants at 280 and 310 K were calculated from the linear plots presented in Fig. 9. (Supporting information). Thus, HKUST-1 has much higher Xe/Kr selectivity at low loading. However, the selectivity in the case of HKUST-1 must drop down rapidly with increasing loading, since the enthalpy of adsorption for Xe decreases much faster, than for Kr, whereas in the case of MFU-4*l* the difference in adsorption enthalpies remains almost the same over the whole measured loading range.

Pressure swing adsorption experiment of Müller et al. also demonstrate the ability of HKUST-1 in noble gas separation [6]. Recently, Ryan et al. in a computational study, investigated the separation of xenon and krypton in several MOFs including HKUST-1. According to their calculations, HKUST-1 showed considerably high performance in Xe/Kr separation [25]. To the best of our knowledge, MFU-4*l* and COF-102 have not been studied for this application previously.

4. Conclusion

In this study, we monitored the interaction strength between different noble gases and microporous frameworks by thermal desorption spectroscopy. TDS results show the high capability of HKUST-1 and MFU-4*l* for the new application of noble gas separation. Further adsorption experiments were employed to determine the isosteric heats of adsorption for Xe and Kr and compare the selectivity of MFU-4*l* and HKUST-1. The results clearly show that

beside HKUST-1, MFU-4*l* can be a potential candidate for noble gas separation. However, to optimize the structure of these materials, a detailed investigation of the preferred adsorption sites is demanded.

Acknowledgments

This work was supported by European FAME master program and German Research Foundation (DFG SPP-1362). The authors thank U. Müller (BASF-SE), R.A. Fischer, Suresh B. Kalidindi, for providing samples.

Appendix A. Supplementary data

Supplementary data associated with this article can be found, in the online version, at http://dx.doi.org/10.1016/j.micromeso.2012.06.004.

References

[1] Z. Bao, S. Alnemrat, L. Yu, I. Vasiliev, Q. Ren, X. Lu, S. Deng, J. Colloid Interface Sci. 357 (2011) 504.
[2] R. Krishna, J.M. van Baten, Phys. Chem. Chem. Phys. 13 (2011) 10593.
[3] Z. Herm, J.A. Swisher, B. Smit, R. Krishna, J.R. Long, Abstr. Pap. Am. Chem. S 241 (2011) 2235.
[4] S.Q. Ma, Pure Appl. Chem. 81 (2009) 2235.
[5] A.C. McKinlay, R.E. Morris, P. Horcajada, G. Férey, R. Gref, P. Couvreur, C. Serre, Angew. Chem. Int. Ed. 49 (2010) 6260.
[6] A.U. Czaja, N. Trukhan, U. Müller, Chem. Soc. Rev. 38 (2009) 1284.
[7] P. Häussinger, R. Glatthaar, W. Rhode, H. Kick, C. Benkmann, J. Weber, H.-J. Wunschel, V. Stenke, E. Leicht, H. Stenger, Ullmann's Encyclopedia of Industrial Chemistry, Wiley VCH Verlag GmbH & Co. KGaA, 2000.
[8] F.G. Kerry, Industrial Gas Handbook: Gas Separation and Purification, CRC Boca Raton, Fla, London, 2007.
[9] K.F. Chackett, D.G. Tuck, Trans. Faraday Soc. 53 (1957) 1652.
[10] C.J. Jameson, A.K. Jameson, H.M. Lim, J. Chem. Phys. 107 (1997) 4364.
[11] P. Ryan, O.K. Farha, L.J. Broadbelt, R.Q. Snurr, AIChE J. 57 (2011) 1759.
[12] P.K. Thallapally, J.W. Grate, R.K. Motkuri, Chem. Commun. 48 (2012) 347.
[13] H.P. U. Mueller, M. Hesse and H. Wessel, German Pattent, in: G. Pattent (Ed.), German Patent, Vol. WO 2005/049892, Germany, 2005.
[14] D. Volkmer, D. Denysenko, M. Grzywa, M. Tonigold, B. Streppel, I. Krkljus, M. Hirscher, E. Mugnaioli, U. Kolb, J. Hanss, Chem. Eur. J. 17 (2011) 1837.
[15] ZIF-8-Basolite® Z1200 CAS Number: 59061–53-9, Sigma Aldrich.
[16] S.B. Kalidindi, K. Yusenko, R.A. Fischer, Chem. Commun. 47 (2011) 8506.
[17] I. Krkljus, M. Hirscher, Microporous Mesoporous Mater. 142 (2011) 725.
[18] B. Panella, M. Hirscher, B. Ludescher, Microporous Mesoporous Mater. 103 (2007) 230.
[19] J.L. Falconer, J.A. Schwarz, Catal. Rev. 25 (1983) 141.
[20] A.G. Wong-Foy, A.J. Matzger, O.M. Yaghi, J. Am. Chem. Soc. 128 (2006) 3494.
[21] T. Yildirim, H. Wu, W. Zhou, J. Am. Chem. Soc. 129 (2007) 5314.
[22] H. Furukawa, O.M. Yaghi, J. Am. Chem. Soc. 131 (2009) 8875.
[23] D. Denysenko, M. Grzywa, M. Tonigold, B. Streppel, I. Krkljus, M. Hirscher, E. Mugnaioli, U. Kolb, J. Hanss, D. Volkmer, Chem. Eur. J. 17 (2011) 1837.
[24] D. Farrusseng, C.c. Daniel, C. Gaudillère, U. Ravon, Y. Schuurman, C. Mirodatos, D. Dubbeldam, H. Frost, R.Q. Snurr, Langmuir 25 (2009) 7383.
[25] R.Q. Snurr, P. Ryan, O.K. Farha, L.J. Broadbelt, AIChE J. 57 (2011) 1759.